Biosensors and Bioelectronics 129 (2019) 64–71

Contents lists available at ScienceDirect

Biosensors and Bioelectronics

journal homepage: www.elsevier.com/locate/bios

2D-porphrinic covalent organic framework-based aptasensor with enhanced photoelectrochemical response for the detection of C-reactive protein

Xi Zhang[1], Kuan-Neng Chi[1], De-Lei Li, Yan Deng, Yu-Chan Ma, Quan-Qing Xu, Rong Hu*, Yun-Hui Yang*

College of Chemistry and Chemical Engineering, Yunnan Normal University, Kunming, Yunnan 650500, PR China

ARTICLE INFO

Keywords:
Porphyrinic covalent organic framework
Photoelectrochemical aptasensor
High photocurrent conversion efficiency
Enhanced photocurrent
C-reactive protein

ABSTRACT

In this study, a novel photoelectrochemical (PEC) aptasensor based on two-dimensional (2D) porphyrinic covalent organic frameworks (p-COFs) for the label-free detection of C-reactive protein (CRP) is presented. The obtained p-COFs possess high conductivity and an improved stability due to strong and rigid covalent linkages. The introduction of p-COFs hinder the recombination of electrons and holes, decreasing their band gap (E_g), thereby which improved the photocurrent conversion efficiency. Compared with pure porphyrin, p-COFs exhibited enhanced photocurrent intensity. An amplified photocurrent conversion efficiency and enhanced photocurrent results from H_2O_2, which act as active molecules and electron donors. As an unprecedented application of COFs in PEC bioanalysis, the detection of CRP with a PEC aptasensor is presented. The assembly of a CRP aptamer on the surface of Ag nanoparticles hinders the electron transfer, resulting in the decrease of the photocurrent response. This PEC aptasensor exhibits good analytical performances such as a rapid response, high stability, wide linear range and excellent selectivity, making COFs promising candidates for PEC bioanalysis.

1. Introduction

Photoelectrochemical (PEC) sensing is a new and promising technique for the detection of biomolecules (Zhao et al., 2014, 2015a, 2015b; Willner et al., 2001; Dai et al., 2016). Compared with conventional electrochemical and optical methods, PEC sensing exhibits potentially higher sensitivity due to the low background signal resulting from the complete separation of excitation source (light) and detection signal (current) (Haddour et al., 2006; Li et al., 2017). PEC sensors integrate the advantages between optical and electrochemical strategies (Zheng et al., 2017). The performance of PEC sensors commonly relies on photoactive substances that produce a photocurrent signal under photoirradiation (Liu et al., 2016a). Currently, many novel materials, such as quantum dots (QDs) (Wen and Ju, 2016), two-dimensional (2D) layered nanostructures (Zhan et al., 2013; Dreyer et al., 2010; Ma and Sasaki, 2015; Tan et al., 2017; Pakdel et al., 2014), organic small molecules (Li et al., 2015) and TiO_2 (Haddour et al., 2006) have been employed as PEC materials. Among them, 2D layered nanostructures have been increasingly researched due to their unique optical and electrical properties resulting from the ultrathin thickness and 2D morphology (Dreyer et al., 2010; Novoselov et al., 2004; Huang et al., 2013; Ma and Sasaki, 2015). Usually, a 2D layered structure is beneficial to shorten charge transport time and distance (Tan et al., 2017), which makes 2D layered nanostructures a brilliant candidate for photoelectrochemical applications. Therefore, exploring 2D materials with high charge transport abilities is highly desirable for the development of PEC sensor.

Until now, a variety of 2D nanomaterials, such as graphene and graphene oxide (Dreyer et al., 2010), nickel sulfide (NiS) (Tan et al., 2017), metal oxides and hydroxides (Ma and Sasaki, 2015) as well as boron nitride (BN) (Pakdel et al., 2014), have been investigated. Among these materials, 2D organic frameworks, including metal-organic frameworks (MOFs) and covalent organic frameworks (COFs), possess highly accessible active sites on their surface, which can be employed for catalytic, electrochemical and sensing applications (Zhao et al., 2015a, 2015b; Campbell et al., 2015; Xu et al., 2015). Recently, Jiang et al. developed porphyrin-based MOFs that showed a significantly enhanced photocatalytic conversion compared with the corresponding porphyrin ligand itself (Xu et al., 2015). Nevertheless, most of the MOFs commonly suffer from low conductivity, poor thermal stability and water tolerance, and they are prone to collapse.

Covalent organic frameworks (COFs), which present organic

* Corresponding authors.
E-mail addresses: hudierong_168@163.com (R. Hu), yyhui2002@aliyun.com (Y.-H. Yang).
[1] These authors made equal contributions to this research.

https://doi.org/10.1016/j.bios.2019.01.009
Received 6 November 2018; Received in revised form 1 January 2019; Accepted 4 January 2019
Available online 15 January 2019
0956-5663/

analogues of MOFs, are a series of crystal organic porous materials with large conjugated architecture and versatile covalently bound organic building units (Côté et al., 2005; Colson et al., 2011; Feng et al., 2012a). Recently, it was demonstrated that p-COFs showed the extraordinary application potentials in gas adsorption, catalysis and semiconductors, because of their specific advantages such as high surface area, high stability and low density (Han et al., 2009). Since the pioneering work of Yaghi in 2005, a growing number of COFs have been synthesized (Côté et al., 2005). Due to their charge transport properties, 2D COFs present a new and promising class of conducting polymers (Spitler and Dichtel, 2010). Banerjee et al. demonstrated that the sensitivity of 2D COFs toward nitroaromatic analytes is about 10-fold higher with respect to bulk COFs (Das et al., 2015). Recently, Jiang et al. reported that π-electron-based Co, Fe, Ni and Mo 2D porphyrinic COFs (p-COFs), which enable high-rate charge-carrier conduction, exhibited outstanding photocatalytic properties (Feng et al., 2012b). Consequently, COFs have great prospect in photoelectric applications. 2D p-COFs, as a photoactive material, would be desirable for PEC applications. In comparison with MOFs, the stability of COFs might be enhanced because of the strong and rigid covalent linkages between the elements (H, C, N and O) resulting from Schiff base condensations. Similar to MOFs, p-COFs could also prolong the electron–hole recombination time under light irradiation, thus promoting the photoelectric conversion efficiency. Therefore, π-electron conjugation, low band gap and active groups make p-COFs ideal materials for the fabrication of PEC-responsive biosensors.

C-reactive protein (CRP) is a highly sensitive marker (acute protein) of infection, inflammation and cardiovascular disease risk (May and Wang, 2007). CRP measurements could provide valuable information for the timely administration of antibiotics and the prediction of the development of cardiovascular diseases (Liu et al., 2016b; Zhang et al., 2016a; Mygind et al., 2011). Up to now, various instrumental methods, such as surface plasmon resonance spectroscopy (Meyer et al., 2006), electrochemical method (Wang et al., 2017a; Liu et al., 2016b) and fluorescence spectroscopy (Islam et al., 2010), have been developed for the rapid and accurate detection of CRP. Among these reported methods, aptamer-based sensors have attracted substantial attention because of their simplicity, high specificity, stability, and relatively low cost. Aptamers are single-stranded DNA or RNA oligonucleotides that are selected in vitro through systematic evolution of ligands by exponential enrichment (SELEX) and can be easily produced using a commercial DNA synthesizer (Pultar et al., 2009; Hu et al., 2014, 2017; Wang et al., 2017b; Gao et al., 2016). Accordingly, the development of an aptamer-based PEC sensor (aptasensor) for the rapid, simple, low-cost, highly sensitive and selective detection of CRP is desirable.

Herein, we developed a novel PEC aptasensor based on p-COFs for the label-free detection of CRP (Scheme 1). The synthesized 2D p-COFs (Scheme 1) with extensive π-conjugation could hinder the recombination of electrons and holes, thereby improving the photocurrent conversion efficiency. Structure and morphology of the p-COFs were characterized by solid state ^{13}C cross-polarization magic-angle spinning (^{13}C NMR), transmission electron microscopy (TEM) and Fourier-transform infrared spectroscopy (FT-IR). The photocurrent intensity of the obtained p-COFs is around three times higher than that of the porphyrin ligand. The improved photocurrent conversion efficiency and photocurrent intensity was further amplified by active molecules, such as H_2O_2, which act as electron donors. An aptamer, which is specifically recognized by CRP, was assembled on the surface of silver nanoparticles (Ag NPs). The introduced CRP hindered the electron transfer, resulting in a decrease of the photocurrent response, which can be employed for the detection of CRP. This work demonstrates the great promise of COFs for the application of PEC bioanalysis, which has, to the best of our knowledge, never been reported.

2. Experimental section

2.1. Materials and reagents

H_2O_2 was purchased from Bohai Chemical Co., Ltd. (Tianjin, China). CRP, chitosan (CHIT) and 5,10,15,20-tetrakis (4-aminophenyl) porphyrin were purchased from Neighbors Biotechnology Co., Ltd. (Shanghai, China). 1,4-Dioxane and 1,3-benzenedialdehyde were obtained from Aladdin Reagent Co., Ltd. (Shanghai, China). Nickel (II) chloride hexahydrate puratrem, thioacetamide (TAA), ethylene glycol and β-mercaptoethanol (MCH) were purchased from Fengchuan Chemical Reagent Co., Ltd. (Tianjin, China). Indium tin oxide (ITO) electrodes were purchased from Tianjin Aida Henghao Technology Development Co., Ltd. (Tianjin, China). CRP aptamer (Sequence: TTT TTC GAA GGG GAT TCG AGG GGT GAT TGC GTG CTC CAT TTG GTG) (Wu et al., 2016) was obtained from Sangon Biotech Co., Ltd. (Shanghai, China). Ultrapure water from a Hitech laboratory water purification system was used in all experiments. All chemicals were of analytical grade.

PEC measurements were performed with PEAC 200 A (Tianjin Aida Heng Sheng Technology Development Co., Ltd., Tianjin, China). All photocurrent experiments were carried out with a conventional three-electrode system on a CHI660D electrochemical workstation (Shanghai Chenhua Instrument Company of Shanghai, China) using the modified ITO electrode as working electrode, a platinum wire as counter electrode and a saturated calomel reference electrode (SCE) as reference electrode unless otherwise stated. Transmission electron microscopy (TEM) was performed using a JEM-200 transmission electron microscope (JEOL, Japan). X-ray diffraction (XRD) measurements were performed using a TTRIII diffractometer (Nippon science Co., Japan).

2.2. Synthesis of p-COFs

p-COFs were synthesized as follows: Briefly, 5,10,15,20-tetrakis(4-aminophenyl)porphyrin (7.5 μmol) and 1,3-benzenedialdehyde (15 μmol) were added to a 20 mL pyrex reaction tube, and the reaction tube was evacuated and sealed with a plastic plug. Then, 1.0 mL 1,4-dioxane was injected into the reaction tube and dissolved ultrasonically, and 0.2 mL acetic acid (3 mol/L) was slowly dropped into the tube. The reaction tube was evacuated by liquid nitrogen cooling to exhaust bubbles and brought to room temperature. Subsequently, the mixture was heated at 95 °C for three days followed by cooling to room temperature. Then, the resulting mixture were collected by centrifugation, and washed three times with tetrahydrofuran (THF) and N, N-dimethylformamide (DMF). After drying in vacuum oven at 60 °C for 12 h, the resulting product was obtained as a brown solid. The p-COFs were highly ultrasonically dispersed before use.

2.3. Synthesis of spherical nickel sulfide (NiS) and Ag NPs

The synthesis of spherical NiS was adopted from a previously published method (Pan et al., 2008). Typically, Nickel (II) chloride hexahydrate puratrem (0.474 g), anhydrous sodium acetate (1.44 g) and thioacetamide (0.15 g) were ultrasonically dissolved in 20 mL ethylene glycol. The mixture was transferred to an autoclave and reacted at 140 °C for 8 h. After cooling to room temperature, the resulting mixture was collected by centrifugation and washed three times with ethanol. After drying in a vacuum, the resulting product was harvested as a black solid.

Ag NPs were synthesized according to a previously reported method (Mulvihill et al., 2010). Firstly, 9 mg silver nitrate were ultrasonically dispersed in 50 mL H_2O and heated at 98 °C under stirring. Then, 1.2 mL (1%) sodium citrate was quickly injected into the solution and heated at 98 °C for 40 min. Finally, the resulting solution was stored in a refrigerator at 4 °C for further use.

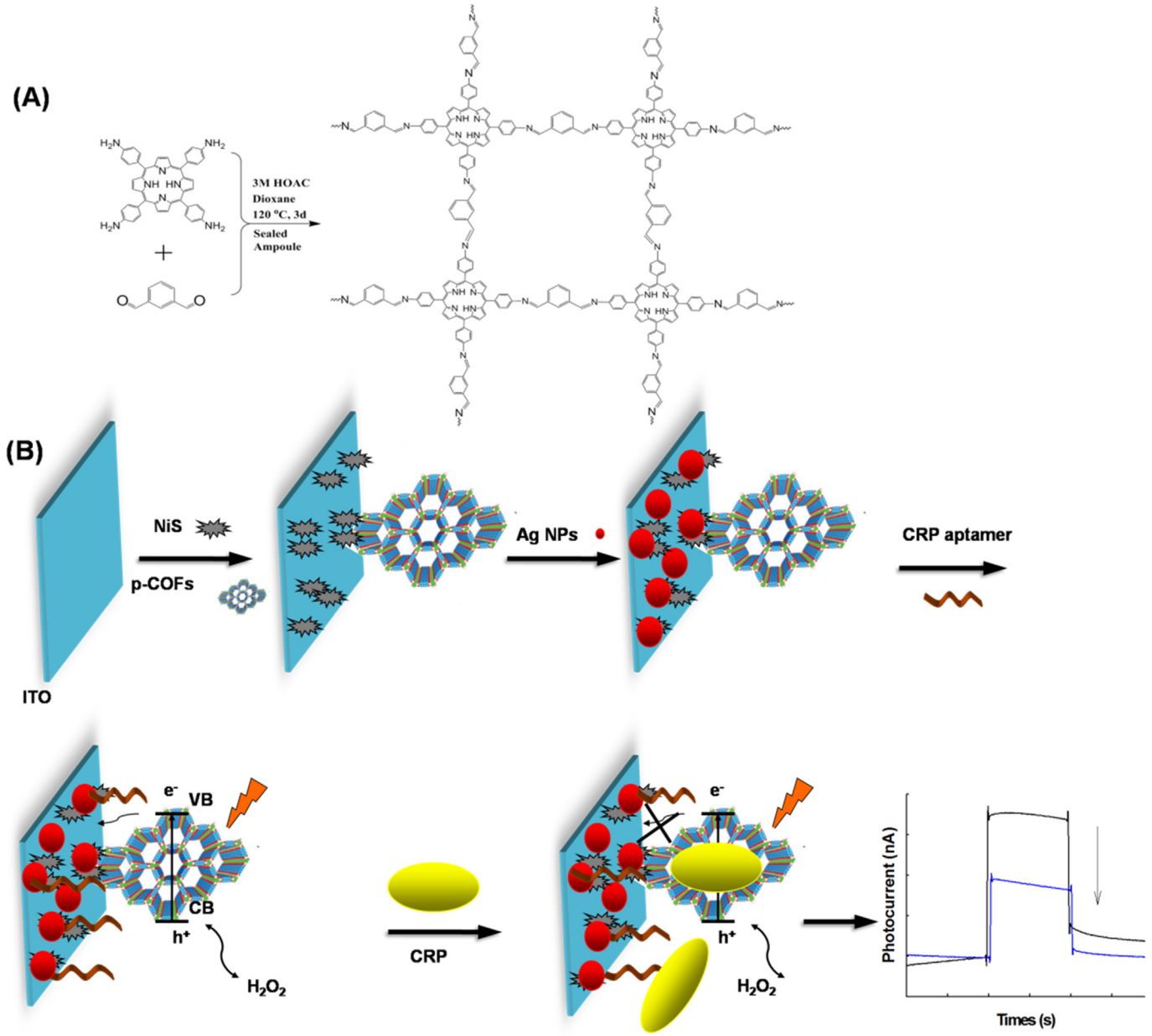

Scheme 1. (A) Preparation of p-COPs by condensation. (B) Procedure for the stepwise fabrication of CRP photoelectrochemical biosensors.

2.4. Fabrication of photoelectrochemical aptasensor

In this work, ITO (5.0 wt% In_2O_3 + SnO_2) was employed for the development of the PEC biosensor. Briefly, ITO electrodes were sonicated in acetone, absolute ethanol and deionized water for 5 min, respectively. After drying at room temperature, 10.0 μL NiS/CHIT (1:1, (v/v)) was dropped onto the clean ITO electrode and dried at room temperature. After washing with distilled water, 10.0 μL p-COFs/CHIT (1 mg/mL; 1:1 (v/v)) was pipetted onto the NiS-modified ITO electrode and dried. After rinsing with distilled water, 10.0 μL Ag NP suspension was dropped onto the resulting ITO electrode. Subsequently, 10.0 μL of a solution of CRP aptamer (0.5 μM) was dropped onto the electrode, which was incubated for 60 min at 37 °C. Finally, the as-prepared sensor was incubated with 1 mM MCH for 30 min at 37 °C. Then, 10 μL of a solution of CRP with different concentrations was dropped onto the aptasensor and incubated for 30 min at 37 °C.

2.5. Measurement procedure

The biosensor was rinsed with 0.1 M phosphate buffer solution (PBS, pH = 7.4). The photocurrent measurement was carried out under optimal conditions in PBS at pH 7.4, and the modified electrode generated a PEC signal.

3. Results and discussion

3.1. Characterization

In order to confirm the successful p-COF synthesis, shape and structure of the samples were analyzed by TEM. As shown in Fig. 1A, the p-COFs exhibited the morphology of a thin flat and slightly wrinkled layer structure. The SEM was also utilized to confirm the shape of p-COFs. As seen in Fig. S1, this result was in accordance with the TEM characterization. FT-IR revealed a strong C=N stretching vibration at 1616–1624 cm^{-1} resulting from imine bonds (Fig. 1B) (Feng et al.,

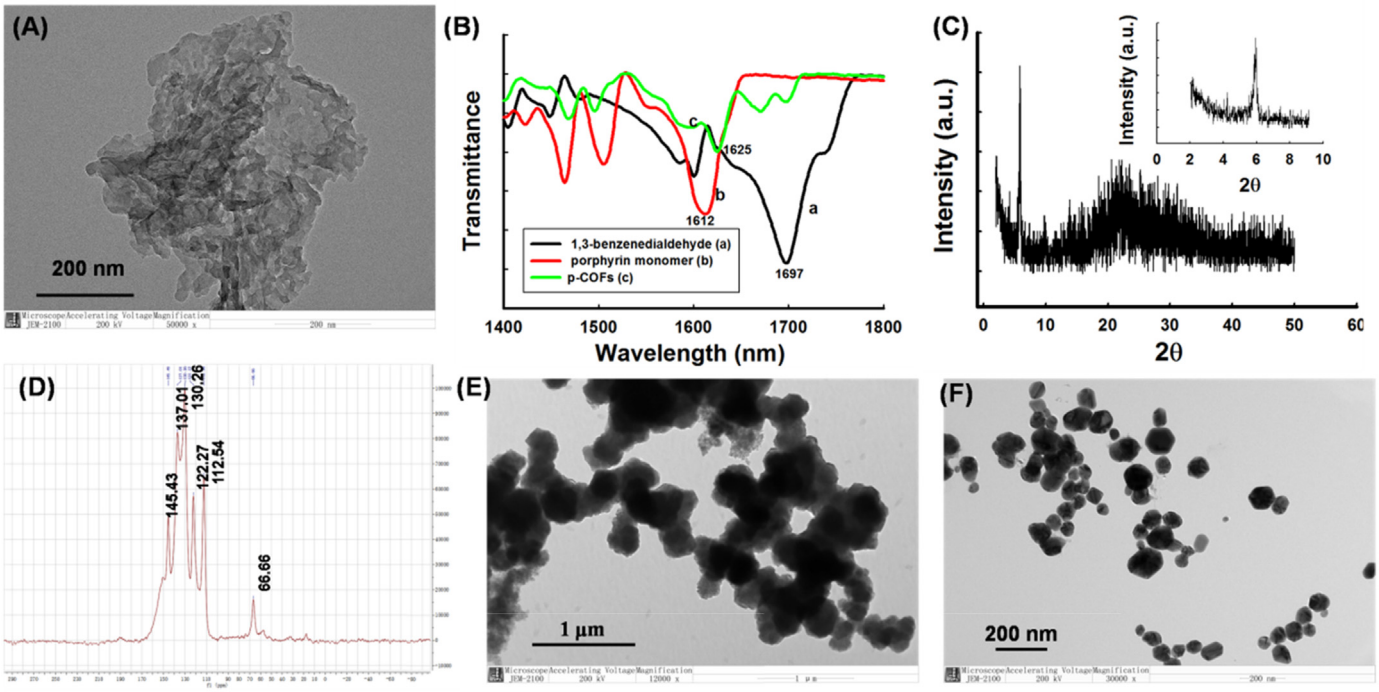

Fig. 1. (A) TEM image of p-COFs; (B) FT–IR spectral profiles of p-COFs; (C) XRD pattern of p-COFs; (D) ^{13}C CP/MAS NMR spectra of p-COFs; (E) TEM image of NiS; (F) TEM image of Ag NPs.

2012b). X-ray diffraction (XRD) shows a strong and sharp diffraction peak (100) at 2θ = 5°, indicating an ordered crystalline COF material (Fig. 1C) (Liu et al., 2016b). The ^{13}C cross-polarization magic-angle spinning (CP/MAS) NMR spectrum peak at ~ 145 ppm corresponds to the carbon atom of the C=N bond, the formation of which is characteristic for the condensation of aldehyde and primary amine (Fig. 1D) (Liu et al., 2016b). The signals at ~ 112, 122, 130 and 137 ppm could be attributed to the carbon atoms of the phenyl groups (Wang et al., 2011). To achieve the highly sensitive detection of CRP, NiS and Ag NPs were also synthesized. Fig. 1E shows the TEM image of NiS. Ag NPs were used for biomolecule conjugation. The prepared Ag NPs have an average diameter of approximately 50–100 nm, as measured by TEM (Fig. 1F). The above results demonstrate that p-COFs, NiS and Ag NPs were successfully synthesized. Moreover, SEM was used to characterize to the modification of the electrode's surface. One can see that the NiS, p-COFs and AgNPs were modified on the electrode by a layer-by-layer way (Fig. S2).

3.2. Mechanism investigations

The spectroscopic properties of COFs were investigated by UV–visible (UV–Vis) and fluorescence (FL) emission spectroscopy. As shown in Fig. 2A, the UV–Vis absorption spectrum of porphyrin monomer in DMF showed an absorption peak at ~ 420 nm (curve a). In contrast, the corresponding peak of p-COFs was red shifted by 18 nm and located at 438 nm (curve b), showing that p-COFs possess smaller HOMO-LUMO gaps. When NiS was continuously added to the p-COFs solution, a 2-nm red shift compared with p-COFs was observed (curve c). In addition, the band gap (E_g) of semiconductors can be calculated by the Kubelka–Munk formula:

$$a = A(h\nu - E_g)^{n/2}/h\nu$$

where a, E_g, A, ν and h are absorption coefficient, band energy, proportionality constant, frequency of the incident light and Planck's constant, respectively. As a result, the E_g values of porphyrin ligand, COFs and NiS-COFs are 2.95, 2.83 and 2.81 eV, respectively.

Fluorescence spectroscopy is a powerful tool to study charge separation and recombination processes in excited semiconductors (Wen et al., 2017). As shown in Fig. 2B, when pure porphyrin ligand and p-COFs were excited at 414 nm, a strong fluorescence peak at 695 nm was detected (curve a and b). Upon the addition of NiS, the fluorescence intensity decreased under the same excitation conditions (curve c), owing to the energy transfer of photoexcited electrons from p-COFs to NiS nanoparticles, thus greatly inhibiting charge recombination. Lower PL intensity indicates a lower recombination efficiency of photogenerated charge carriers, corresponding to a higher amount of photogenerated electrons and holes, which could achieve a higher photocurrent.

The enhanced charge separation efficiency could also be confirmed by the photocurrent response, which is often used to investigate the visible-light PEC performance of the surface of different photocatalysts. As shown in Fig. 2C, the photocurrent intensity of p-COFs is three times higher than that of the porphyrin ligand for the same molar concentration of porphyrin (curve a and b). The p-COFs have a stronger photoelectric conversion ability compared with the porphyrin ligand, indicating p-COFs could effectively suppress radiative electron–hole recombination and thus promote the generation of photogenerated electron–hole pairs. Moreover, dropping p-COFs onto a NiS-modified surface produced a higher photocurrent than when the surface was incubated with porphyrin ligand or p-COFs (curve c). The above results show that the p-COFs photocatalyst has a lower recombination rate and a more efficient charge separation.

Several active molecules such as H_2O_2, p-nitrophenol, dopamine, cysteine and ascorbic acid were selected as electron donors for studying the enhancement of the photocurrent for signal amplification. As displayed in Fig. 2D, in the O_2-saturated environment, the electron donor H_2O_2 produced the highest photocurrent among the active molecules dopamine, ascorbic acid and cysteine (photocurrent intensity: H_2O_2 > p-nitrophenol > dopamine > ascorbic acid > cysteine). Thus, these active molecules improved the photocurrent conversion efficiency and photocurrent intensity.

In order to investigate the electronic band structures of p-COFs, Mott-Schottky (MS) plots were measured to estimate the potential change of the conduction band (CB) edge of the porphyrin ligand and

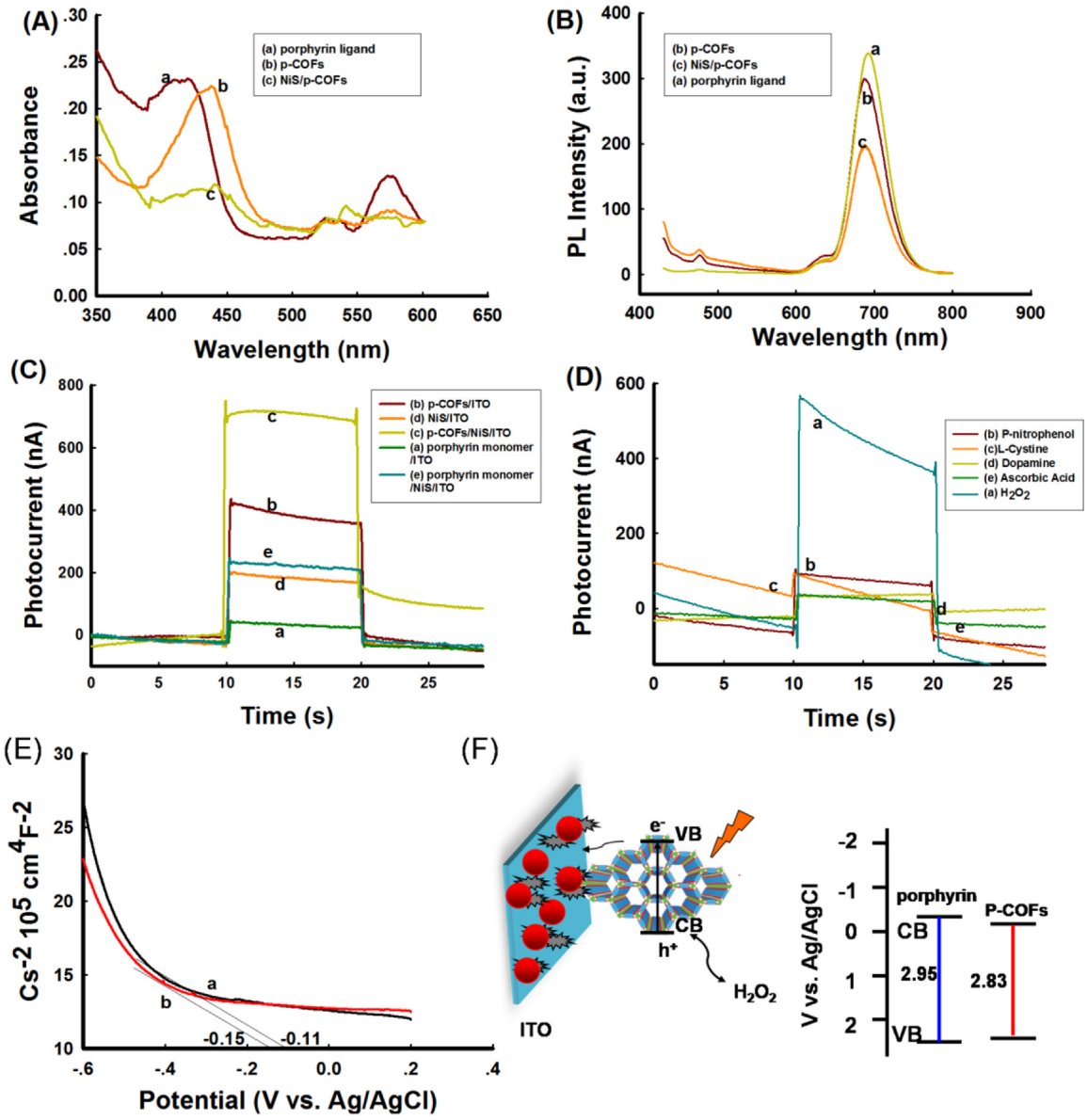

Fig. 2. (A) UV–Vis absorption spectra of porphyrin monomer (a), p-COFs (b), and NiS/p-COFs (c); (B) fluorescence spectra of p-COFs (a), porphyrin monomer (b), and p-COFs in the presence of NiS (c); (C) photocurrent responses of porphyrin monomer/ITO (a), p-COFs/ITO (b), p-COFs/NiS/ITO (c), NiS/ITO (d), and porphyrin monomer/NiS/ITO (e). H_2O_2 concentration 12 mM; (D) photocurrent responses of CRP aptamers/Ag NPs/COFs/NiS/ITO in O_2-saturated buffer solution in the presence of 12 mM H_2O_2 (a), p-nitrophenol (b), cysteine (c), dopamine (d), and ascorbic acid (e). (E) MS plots of p-COFs (a) and porphyrin ligand (b). (F) schematic diagram of the PEC sensor with selectivity to H_2O_2.

the COFs at 1 kHz in Na_2SO_4 solution (0.1 M). As shown in Fig. 2E, the calculated flat-band potentials for the porphyrin ligand and the COFs are –0.15 and −0.11 V (vs. Ag/AgCl), respectively. Thus, the valence band (VB) position could be calculated from the values of CB and E_g. Accordingly, the VB positions for the porphyrin ligand and the COFs were estimated to be 2.60 and 2.52 V (vs. Ag/AgCl), respectively.

Based on our above results, a possible photocatalytic mechanism was proposed, which is presented in Fig. 2F. The p-COFs have a low E_g value, promoting the generation of photogenerated electron–hole pairs. In p-COFs, electrons and holes are generated by visible light, which excites electrons from VB to CB, leaving holes in the VB. NiS is a material with good conductivity, which could promote the generation of photocurrent. Active molecules, such as H_2O_2, that are smaller than the pore apertures of p-COFs can pass through the p-COFs pores. These molecules can be effectively oxidized by photogenerated holes to provide more electrons under light excitation on the surface of the COFs ($H_2O_2 + 2h^+ \rightarrow 2H^+ + O_2$). Then, the remaining electrons are transported to the p-COFs to promote the generation of electron–hole pairs, resulting in an enhanced photocurrent response.

3.3. Characterization of the modified electrode

Electrochemical impedance spectroscopy (EIS) was performed to confirm that the sensing surface was successfully fabricated. Furthermore, EIS is an effective method to investigate the charge transfer process. As shown in Fig. 3A, the bare ITO electrode displays a small R_{et} value (curve a), indicating little impairment of the electron transfer. After surface modification with NiS, the R_{et} value increased slightly (curve b) due to the good conductivity of NiS (Ret = 21 Ω). After addition of p-COFs, the R_{et} value decreased slightly (curve c) compared to that of curve b, revealing that the high charge transfer rate of the p-COFs with the periodic arrays of π clouds is beneficial for the

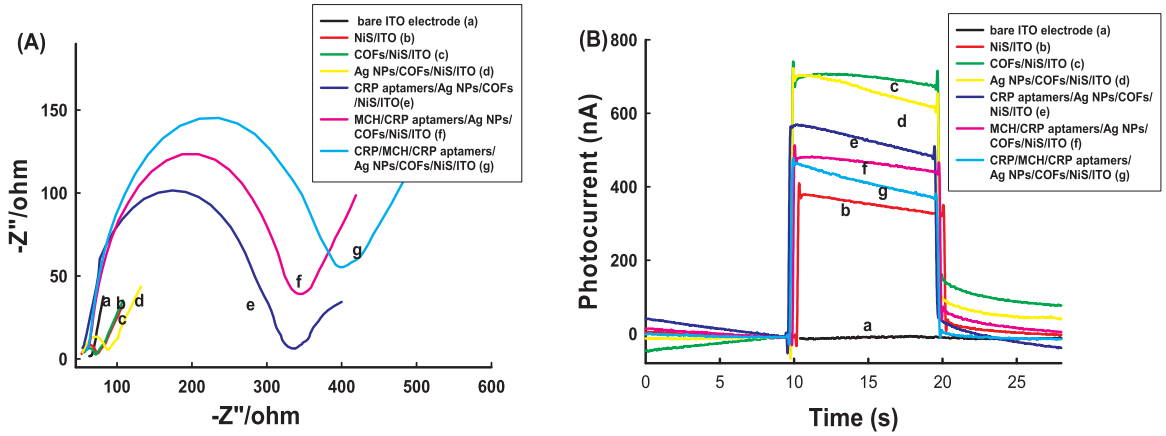

Fig. 3. Electrochemical impedance spectroscopy (A) and photosensitive properties (B) of the bare ITO electrode (a), NiS/ITO (b), COFs/NiS/ITO (c), Ag NPs/COFs/NiS/ITO (d), CRP aptamers/Ag NPs/COFs/NiS/ITO (e), MCH/CRP aptamers/Ag NPs/COFs/NiS/ITO (f) and CRP/MCH/CRP aptamers/Ag NPs/COFs/NiS/ITO (g). EIS spectra were recorded in $Fe(CN_6)^{3-/4-}$ solution containing 0.1 mol/L KCl in the frequency range from 0.1 Hz to 100 kHz. PEC spectra were recorded in 0.1 M phosphate buffer solution (pH = 7.4) under light irradiation. CRP concentrations: 20 nM.

PEC process (Ret = 15 Ω). After incubating the modified ITO electrode with Ag NPs, the R_{et} value increased slightly (curve d) (Ret = 34 Ω). After incubating the modified ITO electrode with CRP aptamer, the impedance increased obviously (curve e), indicating the successful binding of CRP aptamer (Ret = 275 Ω). After incubating the modified electrode with MCH, the impedance increased (curve f) (Ret = 292 Ω). In the presence of target CRP, the impedance increased further (curve g), indicating the successful binding of target CRP to CRP aptamer (Ret = 347 Ω), which proves the successful construction of our sensing surface.

The fabrication process of the PEC sensor was also monitored based on the photocurrent responses. Fig. 3B presents the photocurrent response of the modified ITO electrode in 0.1 M phosphate buffer solution under light irradiation. The bare ITO electrode exhibited no photocurrent signal (curve a), while the NiS/ITO electrode exhibited a strong photocurrent response under light irradiation (curve b). After deposition of p-COFs on the modified electrode, the photocurrent almost doubled because of the good photosensitive properties of the p-COFs (curve c). Ag NPs were used for biomolecule conjugation. The photocurrent decreased slightly after incubation of the modified ITO electrode with Ag NPs (curve d). Afterward, CRP aptamer was linked to the modified electrode, resulting in a further decrease of the photocurrent (curve e), which confirmed the successful binding of the aptamer to the modified electrode, as binding with insulating biomolecules is expected to inhibit the electron transfer. After incubating the modified electrode with MCH, the photocurrent decreased slightly (curve f). In the presence of target CRP, the photocurrent decreased further (curve g). These results confirm the above results obtained by EIS.

3.4. Optimization of conditions

In order to achieve the best sensing performance of the PEC sensor, applied potential, pH of detection solution, H_2O_2 concentration, CRP aptamer incubation time and CRP aptamer concentration were optimized. As shown in Fig. 4A, the photocurrent obviously increased when the detection potential was increased from –0.1 to + 0.7 V, indicating that the external voltage effectively prompted the separation of the photoelectrons from the holes. Thus, 0.7 V was chosen as the detection potential. Simultaneously, the photocurrent of the PEC biosensor showed a maximum at pH 7.5 (Fig. 4B). H_2O_2, which was employed as an electron donor, has a significant effect on the photocurrent response. As shown in Fig. 4C, the photocurrent increased when the H_2O_2 concentration was increased and reached a steady state at a concentration of 12 mM. Moreover, the photocurrent maximum was achieved for a CRP aptamer incubation time of 50 min (Fig. 4D) and a CRP aptamer concentration of 0.5 μM (Fig. 4E). Therefore, these optimized conditions were chosen for further investigations.

3.5. Analytical performance

The photocurrent response was studied for different CRP concentrations under the optimized experimental conditions. As shown in Fig. 5A, the photocurrent decreased with the increase of the CRP concentration. The photocurrent decreased inversely proportional to the target CRP concentration increasing from 0.5 to 100 ng/mL (Fig. 5B). The detection limit (LOD) was estimated to 0.1 ng/mL, determined by the 3δ/slope (δ, standard deviation of the blank samples). The linear regression equation could be fitted as follows: ΔI (nA) = –1.80 c + 362.31 (ng/mL). Such a low detection limit can be attributed to the strong signal amplification of the electron donor H_2O_2 and the p-COFs. Therefore, the sensitivity is comparable to or better than that reported in some previous correlative work (Liu et al., 2016b; Zhang et al., 2016a, 2016b; Wu et al., 2016; Hu et al., 2016; Iwasaki et al., 2014; Ji et al., 2016; Piccoli et al., 2018; Meyer et al., 2006) (Table S1). The photocurrent response of the p-COFs was repeatedly measured at 10 s intervals, and the photocurrent intensity shows a slight but distinct change. The photocurrent intensity of the ITO electrode showed no obvious change after 20 days of storage at 4 °C under darkness, revealing good stability for further PEC bioanalysis applications. This result indicates that the photocurrent intensity of the modified electrode is stable, which is beneficial for the construction of a PEC sensor.

Selectivity is an important factor to evaluate the performance of a biosensor; therefore, instead of CRP, other non-target molecules were added to investigate the selectivity of the biosensor. As these non-target molecules, human chorionic gonadotropin (HCG), prostate specific antigen (PSA), microcystin (MC–LR) and bovine albumin (BSA) were chosen. As shown in Fig. 5C, only CRP (20 ng/mL) caused a dramatic decrease in the photocurrent, while the photocurrent in the presence of any of the other non-target analytes (100 ng/mL) was almost the same as measured with the modified electrode in PBS solution. Even when 100 ng/mL PSA, BSA, HCG or 1000 ng/mL glucose (G) were added together with CRP (20 ng/mL) in 0.1 M PBS (pH 7.4), none of these proteins showed any obvious interference with the detection of CRP (Fig. 5D). This finding demonstrates the excellent selectivity of our PEC biosensor for the detection of CRP over that of other proteins.

3.6. Analysis of CRP in real serum samples

To test the applicability and reliability of the presented strategy, we further detected CRP in serum samples. In order to avoid interference of

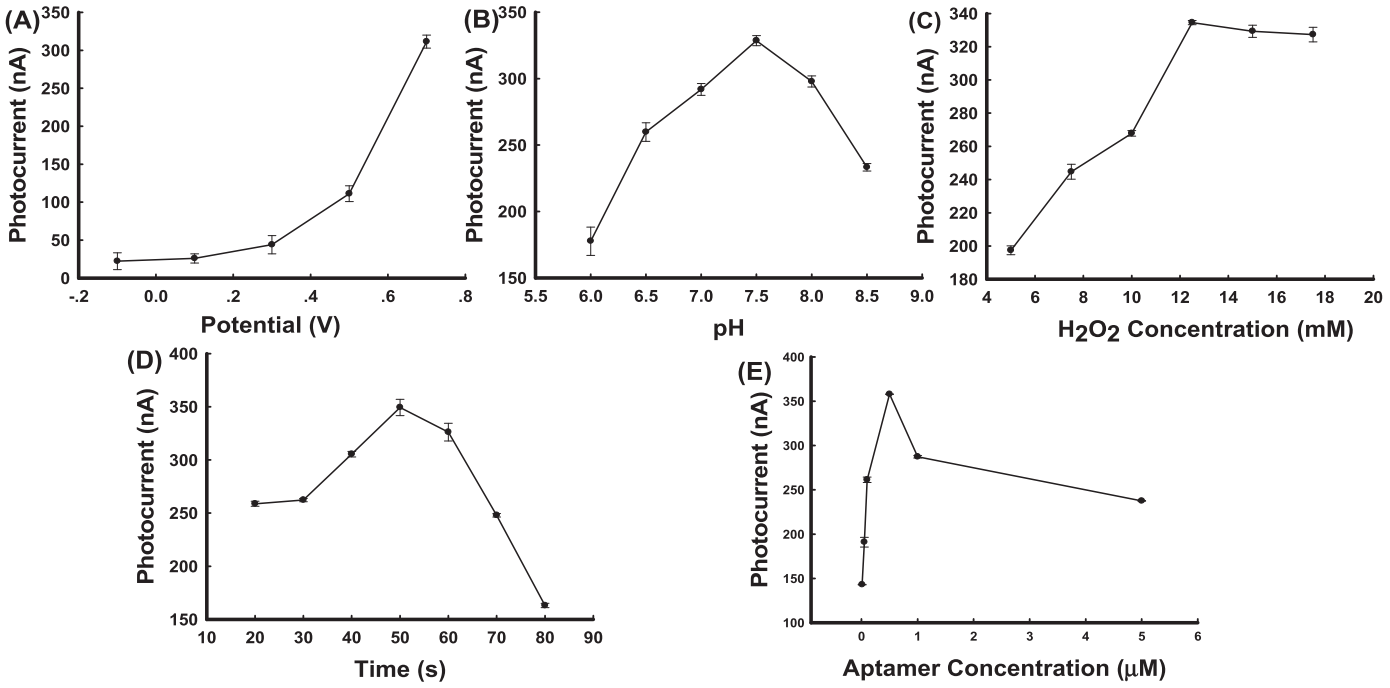

Fig. 4. Effects of the detection potential (A), pH of the detection solution (B), concentration of H_2O_2 (C), CRP aptamer incubation time (D), and CRP aptamer concentration (E). CRP concentration: 0 nM.

the background signal from the serum, varying amounts of CRP were added to diluted 10% serum samples. The analytical results shown in Table S2, which reveal good recovery values for the detection of CRP in real serum samples.

Next, we also studied the reproducibility of the PEC sensor by repeatedly detecting three CRP standards of different concentrations, including 20, 40 and 50 ng/mL. Analysis of our experimental results revealed relative standard deviations (RSD) under the same experimental conditions of 3.97%, 3.02% and 3.71% (n = 3) for the abovementioned three samples, respectively, and the average recovery for all three detections was 100.4%. Thus, the reproducibility of the PEC sensor was satisfactory.

4. Conclusion

In this work, a novel PEC aptasensor based on p-COFs was

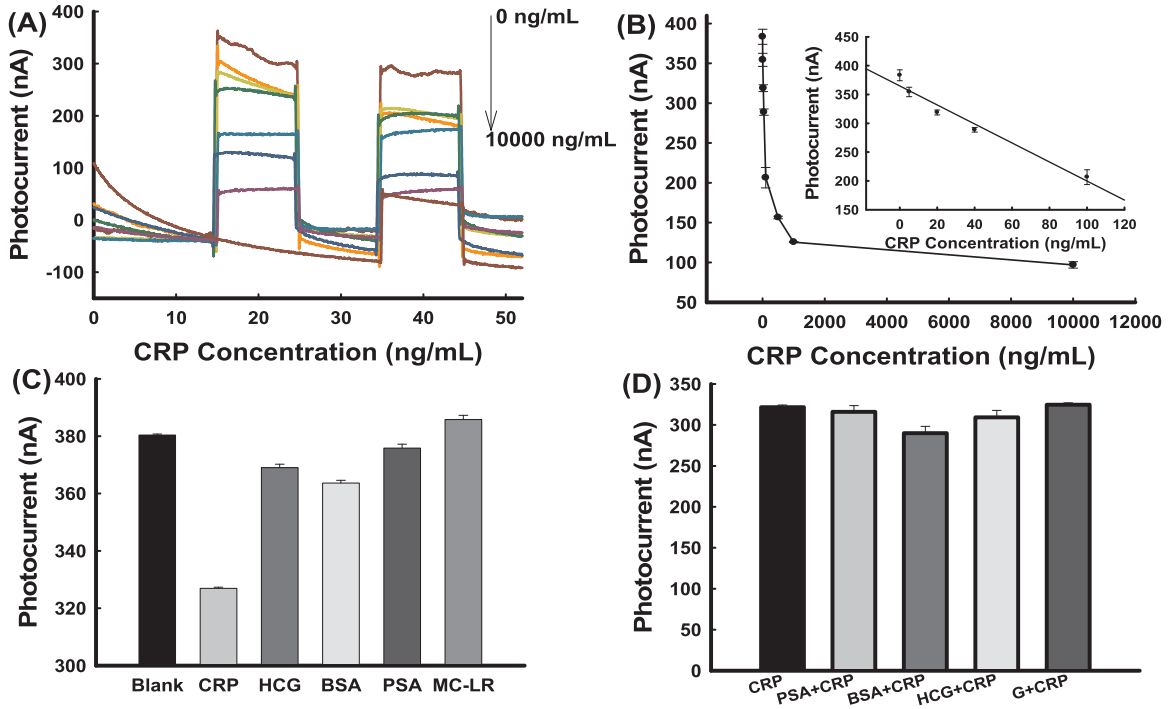

Fig. 5. (A) Photocurrent intensity for different CRP concentrations. (B) Photocurrent change for different CRP concentrations ranging from 0 to 100 ng/mL. The inset is the linear relationship between current intensity and low CRP concentration. (C, D) Specificity of the PEC sensor toward 20 ng/mL CRP, 100 ng/mL HCG, 100 ng/mL PSA, 100 ng/mL MC-LR, 100 ng/mL BSA and 1000 ng/mL G.

developed for the label-free detection of CRP. The p-COFs were prepared through on-step Schiff base condensation and exhibited high conductivity. The p-COFs' stability was enhanced due to strong and rigid covalent linkages. The introduction of p-COFs hindered the recombination of electrons and holes, thereby improving the photocurrent conversion efficiency. Compared with pure porphyrin, p-COFs exhibited enhanced photocurrent intensity. Furthermore, the oxidation of the electron donor H_2O_2 amplified the signal due to the photogeneration of holes upon light excitation. An aptamer, which is specifically recognized by CRP, was assembled on the surface of silver nanoparticles (Ag NPs). The introduced CRP hindered the electron transfer, resulting in a decrease of the photocurrent response, which can be employed for the detection of CRP. These characteristics led to the PEC sensor's high sensitivity and wide potential range that avoids potential interference. The developed PEC aptasensor exhibited a wide linear range (0.5–100 ng/mL) and a low detection limit (0.1 ng/mL). Moreover, the aptasensor could be detect in real serum samples, and the reproducibility of the PEC sensor was satisfactory. To the best of our knowledge, this is the first work to present COFs and their great promise for applications in PEC bioanalysis.

Acknowledgement

This work was supported by the NSFC grants (Grants 21864026, 21605130, 21165023, 21465026, J1210040, 21275044) and theNational Key Scientific Program of China (2011CB911000).

Declaration of interest statement

We declare that we do not have any commercial or associative interest that represents a conflict of interest in connection with the work submitted.

Notes

The authors declare no competing financial interest.

Appendix A. Supporting information

Supplementary data associated with this article can be found in the online version at doi:10.1016/j.bios.2019.01.009.

References

Campbell, M.G., Sheberla, D., Liu, S.F., Swager, T.M., Dinca, M., 2015. Angew. Chem. Int. Ed. 54, 4349–4352.
Côté, A.P., Benin, A.I., Ockwig, N.W., O'Keffe, M., Matzger, A.J., Yaghi, O.M., 2005. Science 310, 1166–1170.
Colson, J.W., Woll, A.R., Mukherjee, A., Levendorf, M.P., Spitler, E.L., Shields, V.B., Spencer, M.G., Park, J., Dichtel, W.R., 2011. Science 332, 228–231.
Das, G., Biswal, B.P., Kandambeth, S., Venkatesh, V., Kaur, G., Addicoat, M., Heine, T., Vermab, S., Banerjee, R., 2015. Chem. Sci. 6, 3931–3939.
Dai, H., Zhang, S., Hong, Z., Lin, Y., 2016. Anal. Chem. 88, 9532–9538.
Dreyer, D.R., Park, S., Bielawski, C.W., Ruoff, R.S., 2010. Chem. Soc. Rev. 39, 228–240.
Feng, X., Ding, X., Jiang, D., 2012a. Chem. Soc. Rev. 41, 6010–6022.
Feng, X., Liu, L., Honsho, Y., Saeki, A., Seki, S., Irle, S., Dong, Y., Nagai, A., Jiang, D., 2012b. Angew. Chem. 124, 2672–2676.
Gao, F., Du, L., Zhang, Y., Zhou, F., Tang, D., 2016. Biosens. Bioelectron. 86, 185–193.
Han, S.S., Mendoza-Cortes, J.L., Goddard, W.A., 2009. Chem. Soc. Rev. 38, 1460–1476.
Haddour, N., Chauvin, J., Gondran, C., Cosnier, S., 2006. J. Am. Chem. Soc. 128, 9693–9698.
Huang, X., Zeng, Z., Zhang, H., 2013. Chem. Soc. Rev. 42, 1934–1947.
Hu, C., Ioannis, Z., Kai, S., Sally, A., Peter, A., Hywel, M., 2016. Anal. Chem. 88, 4872–4878.
Hu, R., Zhang, X., Xu, Q., Lu, D., Yang, Y., Xu, Q., Ruan, Q., Mo, L., Zhang, X., 2017. Biosens. Bioelectron. 92, 40–46.
Hu, R., Zhang, X., Zhao, Z., Zhu, G., Chen, T., Fu, T., Tan, W., 2014. Angew. Chem. Int. Ed. 126, 5931–5936.
Iwasaki, Y., Kimura, T., Orisaka, M., Kawasaki, H., Goda, T., Yusa, S., 2014. Chem. Commun. 50, 5656–5658.
Islam, M.S., Yu, H., Lee, H.G., Kang, S.H., 2010. Biosens. Bioelectron. 26, 1028–1035.
Ji, T., Liu, D., Liu, F., Li, J., Ruan, Q., Song, Y., Tian, T., Zhu, Z., Zhou, L., Lin, H., Yang, C., Wang, D., 2016. Chem. Commun. 52, 8452–8454.
Li, C., Wang, H., Shen, J., Tan, B., 2015. Anal. Chem. 87, 4283–4291.
Li, Y., Zhang, N., Zhao, W., Jiang, D., Xu, J., Chen, H., 2017. Anal. Chem. 89, 4945–4950.
Liu, Y., Yan, K., Zhang, J., 2016a. ACS Appl. Mater. Interfaces 8, 28255–28264.
Liu, T., Hu, R., Zhang, X., Zhang, K., Liu, Y., Zhang, X., Bai, R., Li, D., Yang, Y., 2016b. Anal. Chem. 88, 12516–12523.
Ma, R., Sasaki, T., 2015. Acc. Chem. Res. 4, 136–143.
Meyer, M.H.F., Hartmann, M., Keusgen, M., 2006. Biosens. Bioelectron. 21, 1987–1990.
May, A., Wang, T.J., 2007. Expert Rev. Mol. Diagn. 7, 793–804.
Mygind, N.D., Harutyunyan, M.J., Mathiasen, A.B., Ripa, R.S., Thune, J.J., Gøtze, J.P., Johansen, J.S., Kastrup, J., 2011. Inflamm. Res. 60, 281–287.
Mulvihill, M.J., Ling, X.Y., Henzie, J., Yang, P., 2010. J. Am. Chem. Soc. 132, 268–274.
Novoselov, K.S., Geim, A.K., Morozov, S.V., Jiang, D., Zhang, Y., Dubonos, S.V., Grigorieva, I.V., Firsov, A.A., 2004. Science 306, 666–669.
Pakdel, A., Bando, Y., Golberg, D., 2014. Chem. Soc. Rev. 43, 934–959.
Pan, Q., Huang, K., Ni, S., Yang, F., He, D., 2008. Mater. Res. Bull. 43, 1440–1447.
Pultar, J., Sauer, U., Domnanich, P., Preininger, C., 2009. Biosens. Bioelectron. 24, 1456–1461.
Piccoli, J., Hein, R., El-Sagheer, A.H., Brown, T., Cilli, E.M., Bueno, P.R., Davis, J.J., 2018. Anal. Chem. 90, 3005–3008.
Spitler, E.L., Dichtel, W.R., 2010. Nat. Chem. 2, 672–677.
Tan, C., Cao, X., Wu, X., He, Q., Yang, J., Zhang, X., Chen, J., Zhao, W., Han, S., Nam, G., Sindoro, M., Zhang, H., 2017. Chem. Rev. 117, 6225–6331.
Wang, W., Ding, S.Y., Gao, J., Wang, Q., Zhang, Y., Song, W.G., Su, C.Y., Wang, S., 2011. J. Am. Chem. Soc. 133, 19816–19822.
Wang, J., Guo, J., Zhang, J., Zhang, W., Zhang, Y., 2017a. Biosens. Bioelectron. 95, 100–105.
Wang, C., Qian, Y., Zhang, Y., Meng, S., Wang, S., Li, Y., Gao, F., 2017b. Sens. Actuators B: Chem. 238, 434–440.
Willner, I., Patolsky, F., Wasserman, J., 2001. Angew. Chem. Int. Ed. 40, 1861–1864.
Wen, G., Ju, H., 2016. Anal. Chem. 88, 8339–8345.
Wen, J., Xie, J., Zhang, H., Zhang, A., Liu, Y., Chen, X., Li, X., 2017. ACS Appl. Mater. Interfaces 9, 14031–14042.
Wu, B., Jiang, R., Wang, Q., Huang, J., Yang, X., Wang, K., Li, W., Chen, N., Li, Q., 2016. Chem. Commun. 52, 3568–3571.
Xu, H., Hu, J., Wang, D., Li, Z., Zhang, Q., Luo, Y., Yu, S., Jiang, H., 2015. J. Am. Chem. Soc. 137, 13440–13443.
Zhan, W., Kuang, Q., Zhou, J., Kong, X., Xie, Z., Zheng, L., 2013. J. Am. Chem. Soc. 135, 1926–1933.
Zhao, W.W., Xu, J.J., Chen, H.Y., 2014. Chem. Rev. 114, 7421–7441.
Zhao, W.W., Xu, J.J., Chen, H.Y., 2015a. Chem. Soc. Rev. 44, 729–741.
Zhao, M., Wang, Y., Ma, Q., Huang, Y., Zhang, X., Ping, J., Zhang, Z., Lu, Q., Yu, Y., Xu, H., Zhao, Y., Zhang, H., 2015b. Adv. Mater. 27, 7372–7378.
Zheng, Y., Liang, W., Xiong, C., Zhuo, Y., Chai, Y., Yuan, R., 2017. Anal. Chem. 89, 9445–9451.
Zhang, X., Hu, R., Zhang, K., Bai, R., Li, D., Yang, Y., 2016a. Anal. Methods 8, 6202–6207.
Zhang, N., Ma, Z.Y., Ruan, Y.F., Zhao, W.W., Xu, J.J., Chen, H.Y., 2016b. Anal. Chem. 88, 1990–1994.